AD-A253 536

(1)

DTIC ELECTE AUG 3 1992 S C D

1992

SM Report 92-3

The Effects of Hyperbolic Heat Conduction Around a Dynamically Propagating Crack Tip

J.J. Mason[a]
A.J. Rosakis[b]

Graduate Aeronautical Laboratories
California Institute of Technology
Pasadena, CA 91125

92-19410

[a] Graduate Research Assistant

[b] Associate Professor

92 [illegible] 1 005

The Effects of Hyperbolic Heat Conduction Around a Dynamically Propagating Crack Tip

James J. Mason and Ares J. Rosakis

California Institute of Technology, 105-50, Pasadena, CA 91125

Abstract

Using infrared detectors, Zehnder and Rosakis,[1] Zehnder and Kallivayalil[2] and Mason and Rosakis,[3] have recorded the temperature field around a dynamically propagating crack tip in several metals. At the same time, Tzou[4,5] has suggested that the temperature field around a propagating crack tip might exhibit some of the characteristics of hyperbolic heat conduction. In this paper it is shown, by using a corrected solution of the hyperbolic heat conduction equation for a traveling point source and by using an experimental estimate of the active plastic zone (heat generating zone) at a crack tip, that the effects of hyperbolic heat conduction around a propagating crack tip are not observed for the conditions of the experiments. It is shown that due to the adiabatic conditions at the crack tip the solution of the hyperbolic heat equation is indistinguishable from the solution of the parabolic heat conduction equation for crack propagation in steel. Some features of the solution are examined for conditions other than those in the experiments.

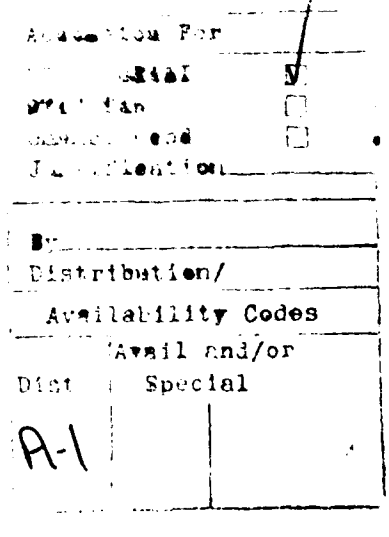

1. Introduction

It is understood that the classical, or parabolic, heat conduction equation has an inherent pathology. That is, when a point source is introduced into a conducting medium, the parabolic heat conduction equation predicts that its presence is instantaneously felt throughout the medium. Often this pathology is referred to as "the infinite speed of heat propagation," and it has been addressed[6] through the introduction of a new heat flux law. Usually, heat flux, $\mathbf{q}$, is related to the gradient of temperature by Fourier's Law,

$$\mathbf{q} = -k\nabla T.$$

When this relation is combined with the expression for the continuity of energy,

$$-\nabla \cdot \mathbf{q} + S = \rho c_p \dot{T},$$

where the dot refers to time differentiation, the parabolic heat conduction equation results,

$$\alpha \nabla^2 T - \dot{T} = -\frac{1}{\rho c_p} S \tag{1.1}$$

(In this paper temperature, T, is implicitly taken as the change in temperature above ambient, $T = T_{\text{actual}} - T_{\text{ambient}}$.) If, instead of Fourier's Law, a new heat flux law is used,

$$\frac{\alpha}{v^2}\dot{\mathbf{q}} + \mathbf{q} = -k\nabla T,$$

then through similar manipulations the "hyperbolic" heat conduction equation results,

$$\alpha \nabla^2 T - \frac{\alpha}{v^2}\ddot{T} - \dot{T} = -\frac{1}{\rho c_p}\left(S + \frac{\alpha}{v^2}\dot{S}\right). \tag{1.2}$$

The introduction of the new heat conduction law has been justified by several authors, (for a review see Tzou[4]) and some experimental work has shown that this different heat conduction equation is more appropriate at large distances from a point source or at very short times after the introduction of a point source.[7] An estimate for the speed of heat propagation in materials, v, may be found,[8] and for steel this estimate predicts a speed of heat propagation on the order of 10^3 m/s.

Zehnder and Rosakis[1] and Mason and Rosa' is[3] have measured the temperature at the tip of a dynamically propagating crack for crack tip velocities ranging from 600 to 900 m/s in 4340 steel. The temperature fields show a strong difference in their geometric nature, see Figure 1, and, since these velocities are comparable to the estimate for the wave speed of heat propagation, it is suggested that this difference may be due to hyperbolic heat conduction. In order to determine whether hyperbolic heat conduction is active in these experiments, it is the purpose of this investigation to produce theoretical temperature fields for the problem of a crack propagating in a hyperbolically conducting metal. It is fundamentally important to note that the propagation of a crack produces plastic deformation at the crack tip and that the plastic work generated during this deformation is mostly transformed into heat. Therefore, the problem of calculating the temperature field around a propagating crack tip is more correctly stated as the problem of calculating the temperature field around a propagating heat source zone with careful attention paid to the boundary conditions at the crack faces.

Several investigations of the temperature field around a propagating crack have been reported for parabolic heat conduction. (For a complete review of this field of work see Mason and Rosakis[3].) The most pertinent here is the work of Weichert and Schonert.[9] These authors numerically calculated the temperature fields around propagating heat source zones by integrating the solution of the parabolic heat conduction equation for a travelling point source over a rectangular heat source zone of constant magnitude. A similar methodology is used here. It should be noted that in all theoretical investigations of the temperature field around a propagating crack tip the assumptions made about the plastic work zone and, consequently, the heat source zone have proven to be extremely important in the calculation of maximum temperature. Due to the complexity of the three dimensional deformation where temperature measurements are performed (at the surface of the specimen), it is difficult to accurately describe the plastic work zone in closed form and most assumptions result in an oversimplification of the experimental problem. Consequently, in this work the shape of the plastic work zone is estimated from the experiments of Zehnder and Rosakis[1] and Mason and Rosakis[3] directly, eliminating over-simplification and, thus, more closely approximating the experimental data.

2. Theoretical Development

First it is necessary to find the solution of the hyperbolic heat conduction equation for a

point source travelling at constant velocity. Although earlier attempts to provide solutions of Eq (1.2) for a traveling point source exist,[10,11] the solution given here includes some corrections that significantly alter the behavior of the solution.

We are interested in solving the equation,

$$\nabla_z^2 T - \frac{1}{v^2}\ddot{T} - \frac{1}{\alpha}\dot{T} = -\frac{1}{\rho c_p \alpha}\left[S(z_1 - \dot{a}t, z_2) + \frac{\alpha}{v^2}\dot{S}(z_1 - \dot{a}t, z_2)\right], \tag{2.1}$$

for a point source travelling at a constant velocity, $\dot{a}$, in the z_1 direction, i.e.

$$S(z_1 - \dot{a}t, z_2) = \delta(z_1 - \dot{a}t)\delta(z_2).$$

Substituting for $S(z_1 - \dot{a}t, z_2)$, Eq (2.1) becomes:

$$\nabla_z^2 T - \frac{1}{v^2}\ddot{T} - \frac{1}{\alpha}\dot{T} = -\frac{1}{\rho c_p \alpha}\left[\delta(z_1 - \dot{a}t)\delta(z_2) + \frac{\alpha}{v^2}\frac{\partial\delta(z_1 - \dot{a}t)}{\partial t}\delta(z_2)\right]. \tag{2.2}$$

It may be shown that the solution of this equation depends upon M^2, where $M = \dot{a}/v$, and that this dependence may be divided into three regimes, $M^2 < 1$, $M^2 = 1$ and $M^2 > 1$. The former and latter cases will be addressed here.

2.1 For the case $M^2 < 1$

By employing the transformation,

$$\xi_1 = \frac{z_1 - \dot{a}t}{\sqrt{1 - M^2}},$$
$$\xi_2 = z_2$$

equation (2.2) may be expressed as

$$\nabla_\xi^2 T + \frac{\dot{a}}{\alpha\sqrt{1 - M^2}}\frac{\partial T}{\partial \xi_1} = -\frac{1}{\rho c_p \alpha}\left[\delta(\xi_1\sqrt{1 - M^2})\delta(\xi_2) - \frac{\alpha M^2}{\dot{a}\sqrt{1 - M^2}}\frac{\partial\delta(\xi_1\sqrt{1 - M^2})}{\partial\xi_1}\delta(\xi_2)\right]. \tag{2.3}$$

We guess a solution to Eq (2.3) of the form

$$T_p(\xi_1, \xi_2) = \exp[-\kappa\xi_1]\, f(\xi_1, \xi_2) \tag{2.4}$$

where

$$\kappa = \frac{\dot{a}}{2\alpha\sqrt{1 - M^2}}$$

which when inserted in equation (2.3) yields

$$\nabla_\xi^2 f - \kappa^2 f = -\frac{1}{\rho c_p \alpha}\exp[\kappa\xi_1]\left\{\delta(\xi_1\sqrt{1-M^2})\delta(\xi_2) - \frac{\alpha M^2}{\dot{a}\sqrt{1-M^2}}\frac{\partial\delta(\xi_1\sqrt{1-M^2})}{\partial\xi_1}\delta(\xi_2)\right\}. \tag{2.5}$$

The left hand side of Eq (2.5) is the modified Helmholtz equation. The Green's function solution of this equation is given by Arfken,[12]

$$G(\mathbf{r}^\xi, \mathbf{r}^\zeta) = -\frac{1}{2\pi}K_0(\kappa|\mathbf{r}^\xi - \mathbf{r}^\zeta|) \tag{2.6}$$

where $K_0(w)$ is the zeroth order modified Bessel's function of the second kind and

$$|\mathbf{r}^\xi - \mathbf{r}^\zeta| = \sqrt{(\xi_1-\zeta_1)^2 + (\xi_2-\zeta_2)^2}.$$

The first vector, $\mathbf{r}^\xi$ refers to the point of interest while the second vector, $\mathbf{r}^\zeta$, refers to the location of the point source. Using the Green's function for the modified Helmholtz equation, the solution to equation (2.5) may be found,

$$\begin{aligned} f(\xi_1,\xi_2) =& \frac{1}{2\pi\rho c_p\alpha}\int_{A^\zeta} K_0(\kappa|\mathbf{r}^\xi - \mathbf{r}^\zeta|)\exp[\kappa\zeta_1]\,\delta(\zeta_1\sqrt{1-M^2})\delta(\zeta_2)d\zeta_1 d\zeta_2 \\ &- \frac{1}{2\pi\rho c_p\alpha}\frac{\alpha M^2}{\dot{a}\sqrt{1-M^2}}\int_{A^\zeta} K_0(\kappa|\mathbf{r}^\xi - \mathbf{r}^\zeta|)\exp[\kappa\zeta_1]\frac{\partial\delta(\zeta_1\sqrt{1-M^2})}{\partial\zeta_1}\delta(\zeta_2)d\zeta_1 d\zeta_2. \end{aligned} \tag{2.7}$$

Equation (2.7) may be divided into two integrals

$$f(\xi_1,\xi_2) = \frac{1}{2\pi\rho c_p\alpha}\left(J_1(\xi_1,\xi_2) + J_2(\xi_1,\xi_2)\right) \tag{2.8}$$

The first of these integrals is found using the fundamental property of the Dirac delta function,

$$J_1(\xi_1,\xi_2) = \frac{K_0(\kappa|\mathbf{r}^\xi|)}{\sqrt{1-M^2}}, \tag{2.9}$$

and the second may be found using the relation

$$\int G(\xi_1,\xi_2,\zeta_1,\zeta_2)\frac{\partial\delta(\zeta_1)}{\partial\zeta_1}\delta(\zeta_2)d\zeta_1 d\zeta_2 = -\left\{\frac{\partial G(\xi_1,\xi_2,\zeta_1,\zeta_2)}{\partial\zeta_1}\right\}_{\zeta_1=0,\zeta_2=0},$$

i.e.

$$J_2(\xi_1,\xi_2) = \frac{M^2}{2(1-M^2)^{3/2}}\left\{K_0(\kappa|\mathbf{r}^\xi|) + \frac{\xi_1}{|\mathbf{r}^\xi|}K_1(\kappa|\mathbf{r}^\xi|)\right\} \tag{2.10}$$

Substituting Eqs (2.9) and (2.10) into Eq (2.8) gives the result

$$f(\xi_1,\xi_2) == \frac{1}{4\pi\rho c_p\alpha(1-M^2)^{3/2}}\left\{(2-M^2)K_0(\kappa|\mathbf{r}^\xi|)+M^2\frac{\xi_1}{|\mathbf{r}^\xi|}K_1(\kappa|\mathbf{r}^\xi|)\right\} \tag{2.11}$$

Remembering our intial guess for temperature in Eq (2.4), we arrive at the solution to Eq (2.3),

$$T_p(\xi_1,\xi_2)=\frac{1}{4\pi\rho c_p\alpha(1-M^2)^{3/2}}\exp\left[-\kappa\xi_1\right]\left\{(2-M^2)K_0(\kappa|\mathbf{r}^\xi|)+M^2\frac{\xi_1}{|\mathbf{r}^\xi|}K_1(\kappa|\mathbf{r}^\xi|)\right\}, \tag{2.12}$$

where

$$|\mathbf{r}^\xi|=\sqrt{\xi_1^2+\xi_2^2}.$$

This is the solution for hyperbolic two dimensional heat flow around a point source traveling in a straight line at a constant speed, $\dot{a} < v$, in an infinite body with $T = 0$ as $r \to \infty$. As $M^2 \to 0$ this function gives the solution of Carslaw and Jaeger[13] for a traveling point source in a parabolically conducting material under identical boundary conditions. This solution differs from the solution provided by Tzou [10,11] due to the interpretation of the argument of the modified Bessel's function in Eq (2.6). In the work by Tzou, it appears that the argument of the modified Bessel's function had been interpreted as the difference of the magnitudes of two vectors where it is actually the magnitude of the difference of two vectors. The additional multiplier of the second term, $\xi_1/|\mathbf{r}^\xi|$, provides desirable behavior for the point source solution not found in the expressions provided by Tzou. Note that using the transformation of coordinates in Eq (2.1) yields

$$\nabla_\xi^2 T+\frac{\dot{a}}{\alpha\sqrt{1-M^2}}\frac{\partial T}{\partial\xi_1}=-\frac{1}{\rho c_p\alpha}\left[S(\xi_1\sqrt{1-M^2},\xi_2)-\frac{\alpha M^2}{\dot{a}\sqrt{1-M^2}}\frac{\partial S(\xi_1\sqrt{1-M^2},\xi_2)}{\partial\xi_1}\right]. \tag{2.13}$$

and that if the slope of the source zone, $S(\xi_1\sqrt{1-M^2},\xi_2)$, is negative in the ξ_1 direction there is a heating contribution due to the second forcing term; if the slope of the source zone in the ξ_1 direction is positive, there is a cooling contribution. The slope of a Dirac delta function in the ξ_1 direction is negative infinite for positive ξ_1 and positive infinite for ξ_1 less that zero.[14] Consequently, it is expected that there should be a heating contribution ahead of the point source that transforms to a cooling contribution behind the point source. The $\xi_1/|\mathbf{r}^\xi|$ term changes the sign of the second term in the solution to produce this behavior.

On the crack faces it is expected that the heat flux out of the material is zero, that is,

$$q_2 = 0\begin{cases}\text{for } \xi_2 = 0^+ \text{ and } \xi_1 \le 0;\\ \text{for } \xi_2 = 0^- \text{ and } \xi_1 \le 0.\end{cases} \tag{2.14}$$

Naturally, this is an idealization of the actual boundary condition which would involve radiation transfer, convective transfer etc. However, it is clear that a fixed temperature over the entire crack faces is not an appropriate boundary condition and is not included in this analysis. In parabolic heat conduction, symmetry of the temperature solution about the x_1 axis is sufficient to satisfy the boundary condition at the crack faces given by Eq (2.14),

$$-k\frac{\partial T}{\partial \xi_2}\bigg|_{\xi_2=0} = q_2(\xi_1, 0) = 0.$$

However, for hyperbolic heat conduction the symmetry results in a first order differential equation, namely,

$$\frac{-\dot{a}a}{v^2\sqrt{1-M^2}}\frac{\partial q_2}{\partial \xi_1}\bigg|_{\xi_2=0} + q_2(\xi_1, 0) = 0$$

It is obvious from Eq (2.14) that $q_2 = 0$ is the solution to this equation. However, it is also clear that the possibility exists for other flow conditions to be prescribed on the crack faces if boundary conditions other than Eq (2.14) exist. In hyperbolic heat conduction symmetry about the ξ_1 axes does not, by itself, imply that q_2 is identically zero on the ξ_1 axis.

2.2 For the case $M^2 > 1$

By employing the transformation,

$$\xi_1 = \frac{z_1 - \dot{a}t}{\sqrt{M^2-1}},$$
$$\xi_2 = z_2$$

Eq (2.2) may be reformulated as

$$-\frac{\partial^2 T}{\partial \xi_1^2} + \frac{\partial^2 T}{\partial \xi_2^2} + \frac{\dot{a}}{a\sqrt{M^2-1}}\frac{\partial T}{\partial \xi_1} = -\frac{1}{\rho c_p a}\left[\delta(\xi_1\sqrt{M^2-1})\delta(\xi_2) - \frac{aM^2}{\dot{a}\sqrt{M^2-1}}\frac{\partial \delta(\xi_1\sqrt{M^2-1})}{\partial \xi_1}\delta(\xi_2)\right]. \tag{2.15}$$

We guess a solution to Eq (2.15) of the form

$$T_p(\xi_1, \xi_2) = \exp[\kappa\xi_1]\, f(\xi_1, \xi_2) \tag{2.16}$$

where

$$\kappa = \frac{\dot{a}}{2a\sqrt{M^2-1}}$$

and substitute above resulting in

$$\frac{\partial^2 f}{\partial \xi_1^2} - \frac{\partial^2 f}{\partial \xi_2^2} - \kappa^2 f = \frac{1}{\rho c_p \alpha} \exp[-\kappa \xi_1] \left\{ \delta(\xi_1 \sqrt{M^2-1}) \delta(\xi_2) - \frac{\alpha M^2}{\dot{a}\sqrt{M^2-1}} \frac{\partial \delta(\xi_1 \sqrt{M^2-1})}{\partial \xi_1} \delta(\xi_2) \right\} \tag{2.17}$$

The left hand side of this equation is the telegraph equation. The Green's function for this equation may be found in Duff and Naylor[15]

$$G(\mathbf{r}^\xi, \mathbf{r}^\zeta) = \frac{1}{2} I_0(\kappa |\mathbf{r}^\xi - \mathbf{r}^\zeta|) H(|\mathbf{r}^\xi - \mathbf{r}^\zeta|^2) H(\zeta_1 - \xi_1) \tag{2.18}$$

where I_0 is the zeroth order modified Bessel function of the first kind, $H(x)$ is the Heaviside function and

$$|\mathbf{r}^\xi - \mathbf{r}^\zeta| = \sqrt{(\xi_1 - \zeta_1)^2 - (\xi_2 - \zeta_2)^2}.$$

Because of the Heaviside terms, the solution in Eq (2.18) is zero outside a triangular regime behind the point source. There exists another Green's function that is non-zero ahead of the point source, but this function is not used due to obvious physical arguments. Because the point source is travelling faster than the wave speed of heat propagation in the material, it is physically impossible to have a finite temperature ahead of the point source. Also, due to the Heaviside terms, the temperature exhibits a jump or shock along lines inclined at an angle ω to the negative ξ_1 axis. The shock angle, ω, is given by the familiar formula,

$$\omega = \pm \sin^{-1}(1/M). \tag{2.19}$$

Not surprisingly, these thermal shocks are quite similar to the shocks found in super-sonic fluid flow. This is to be expected since Eq (1.2) is, in fact, the damped wave equation.

Convolution of the Green's function for the telegraph equation with the forcing term in Eq (2.15) results in two integrals. As before, the first of these integrals is found using the fundamental property of the Dirac delta function,

$$J_1(\xi_1, \xi_2) = \frac{I_0(\kappa |\mathbf{r}^\xi|)}{\sqrt{M^2-1}} . H(|\mathbf{r}^\xi|^2) H(-\xi_1)$$

The second integral is found using the additional relation $\delta(x-c)\delta(x) = 0$,

$$J_2(\xi_1, \xi_2) = -\frac{M^2}{2(M^2-1)^{3/2}} \left\{ I_0(\kappa |\mathbf{r}^\xi|) + \frac{\xi_1}{|\mathbf{r}^\xi|} I_1(\kappa |\mathbf{r}^\xi|) \right\} H(|\mathbf{r}^\xi|^2) H(-\xi_1).$$

Combining these two gives the result

$$f(\xi_1,\xi_2)=\frac{1}{4\rho c_p\alpha(M^2-1)^{3/2}}\left\{(M^2-2)I_0(\kappa|\mathbf{r}^\xi|)-M^2\frac{\xi_1}{|\mathbf{r}^\xi|}I_1(\kappa|\mathbf{r}^\xi|)\right\}H(|\mathbf{r}^\xi|^2)H(-\xi_1).$$

Remembering our intial guess for temperature in Eq (2.16), we arrive at the final result,

$$\begin{aligned}T_p(\xi_1,\xi_2)=&\frac{1}{4\rho c_p\alpha(M^2-1)^{3/2}}\exp[\kappa\xi_1]\\&\left\{(M^2-2)I_0(\kappa|\mathbf{r}^\xi|)-M^2\frac{\xi_1}{|\mathbf{r}^\xi|}I_1(\kappa|\mathbf{r}^\xi|)\right\}H(|\mathbf{r}^\xi|^2)H(-\xi_1).\end{aligned}\tag{2.20}$$

This is the solution of Eq (2.3) for a point source travelling at constant velocity with $M^2>1$. It differs significantly from the solution reported by Tzou[10,11] due to the use of the correct Green's function solution for the telegraph equation. It must be re-emphasized that the definition of the argument of the modified Bessel's functions, $|\mathbf{r}^\xi|$, is significantly different in this case than in the previous case, and, furthermore, that the sign of the argument of the leading exponential term has changed. Although the two solutions appear similar, they are, in fact, not very similar at all; for example, this solution does not converge to the solution of Carslaw and Jaeger[13] under any circumstances. Note the effect of the cooling term in the forcing function on the right hand side of equation (2.15), when $M^2<2$ the temperature at the location of the point source is negative due to the fact that $I_1(w)\to 0$ as $w\to 0$ while $I_0(w)\to 1$ as $w\to 0$. If the cooling term in the forcing function of Eq (2.15) were neglected this effect would not be observed. When $M^2>2$, the solution is always positive.

2.3 Integration over the Source Zone

For the sake of simplicity the heat source zone, $S(\xi_1,\xi_2)$, has been assumed to be defined only on the rectangle $\xi_1\in[0,\delta/\sqrt{1-M^2}]$ and $\xi_2\in[-f\delta,f\delta]$ where f is the aspect ratio of the zone; elsewhere it is identically zero. From the experimental work of Zehnder and Rosakis[1] and Mason and Rosakis[3] it is seen that a close approximation to the experimental heat source zone is given by

$$\frac{S(\xi_1,\xi_2)}{Q}=\frac{1}{2f}\left[1-\cos\left(\frac{2\pi\sqrt{1-M^2}\xi_1}{\delta}\right)\right]\left[1+\cos\left(\frac{\pi\xi_2}{f\delta}\right)\right].$$

where $f = 0.05$. A comparison of the approximate plastic zone, $S(\xi_1, \xi_2)$, with the experimentally estimated plastic zone is shown in Figure 2 for both testing conditions . The inclusion of $1/2f$ in the denominator gives this function characteristics of a Dirac delta function in the ξ_2 (or x_2, given below) direction as $f \to 0$. Consequently, this function is also normalized so that its integral in two dimensions is unity giving usable results if f is allowed to be zero. The multiplier, Q, is found experimentally from the maximum value of the work rate density and the relation between Q and the maximum of the function,

$$Q = \frac{fQ_{max}}{2}.$$

Once this relation for the heat source zone has been assumed, letting

$$\begin{aligned} x_1 = \zeta_1 &= \sqrt{1 - M^2}\frac{\xi_1}{\delta}, \\ x_2 = \zeta_2 &= \frac{\xi_2}{\delta}. \end{aligned} \tag{2.21}$$

the temperature field due to the heat source zone ahead of a crack tip may be found by a convolution;

$$T(x_1, x_2) = Q\delta^2 \int_0^1 \int_{-f}^{f} \frac{S(\zeta_1, \zeta_2)}{Q} T_p(x_1 - \zeta_1, x_2 - \zeta_2) d\zeta_2 d\zeta_1,$$

or, more specifically, for $M^2 < 1$

$$\begin{aligned} T(x_1, x_2) = &\frac{Q\delta^2}{4\pi\rho c_p \alpha (1 - M^2)^{3/2}} \\ &\int_0^1 \int_{-f}^{f} \frac{S(\zeta_1, \zeta_2)}{Q} \exp\left[\frac{-\psi(x_1 - \zeta_1)}{1 - M^2}\right] \\ &\left\{(2 - M^2) K_0\left(\frac{\psi|\mathbf{r}^{\mathbf{x}} - \mathbf{r}^{\zeta}|}{1 - M^2}\right) + M^2 \frac{(x_1 - \zeta_1)}{|\mathbf{r}^{\mathbf{x}} - \mathbf{r}^{\zeta}|} K_1\left(\frac{\psi|\mathbf{r}^{\mathbf{x}} - \mathbf{r}^{\zeta}|}{1 - M^2}\right)\right\} d\zeta_2 d\zeta_1. \end{aligned} \tag{2.22a}$$

where

$$\begin{aligned} \psi &= \frac{\dot{a}\delta}{2\alpha} \\ |\mathbf{r}^{\mathbf{x}} - \mathbf{r}^{\zeta}| &= \sqrt{(x_1 - \zeta_1)^2 + (1 - M^2)(x_2 - \zeta_2)^2} \end{aligned}. \tag{2.22b}$$

Normalizing temperature with respect to $Q\delta/\rho c_p \dot{a}$ for numerical integration yields

$$\begin{aligned} \theta(x_1, x_2) = \frac{\rho c_p \dot{a}}{Q\delta} T(x_1, x_2) = &\frac{\psi}{2\pi(1 - M^2)^{3/2}} \int_0^1 \int_{-f}^{f} \frac{S(\zeta_1, \zeta_2)}{Q} \exp\left[\frac{-\psi(x_1 - \zeta_1)}{1 - M^2}\right] \\ &\left\{(2 - M^2) K_0\left(\frac{\psi|\mathbf{r}^{\mathbf{x}} - \mathbf{r}^{\zeta}|}{1 - M^2}\right) + M^2 \frac{(x_1 - \zeta_1)}{|\mathbf{r}^{\mathbf{x}} - \mathbf{r}^{\zeta}|} K_1\left(\frac{\psi|\mathbf{r}^{\mathbf{x}} - \mathbf{r}^{\zeta}|}{1 - M^2}\right)\right\} d\zeta_2 d\zeta_1. \end{aligned} \tag{2.23a}$$

Similarly for $M^2 > 1$

$$\theta(x_1, x_2) = \frac{\psi}{2(M^2-1)^{3/2}} \int_0^1 \int_{-f}^{f} \frac{S(\zeta_1, \zeta_2)}{Q} \exp\left[\frac{-\psi(x_1-\zeta_1)}{M^2-1}\right] \left\{(M^2-2) I_0\left(\frac{\psi|\mathbf{r}^{\mathbf{x}} - \mathbf{r}^{\zeta}|}{M^2-1}\right) - M^2 \frac{(x_1-\zeta_1)}{|\mathbf{r}^{\mathbf{x}} - \mathbf{r}^{\zeta}|} I_1\left(\frac{\psi|\mathbf{r}^{\mathbf{x}} - \mathbf{r}^{\zeta}|}{M^2-1}\right)\right\} H(|\mathbf{r}^{\mathbf{x}} - \mathbf{r}^{\zeta}|^2) H(-x_1+\zeta_1) . d\zeta_2 d\zeta_1 . \tag{2.24b}$$

Numerical integration of the solution for $M^2 < 1$ proceeds without avail. The singularity in the modified Bessel's function of the zeroth order at the origin is logarithmic, therefore the integral is finite. The singularity in the modified Bessel's function of the first order at the same point is of order $1/|\mathbf{r}^{\mathbf{x}} - \mathbf{r}^{\zeta}|$ which is integrable in two dimensions. (This is easily shown by a conversion to polar coordinates.) Multiplication of $K_1(\psi|\mathbf{r}^{\mathbf{x}} - \mathbf{r}^{\zeta}|)$ by the factor $(x_1 - \zeta_1)/|\mathbf{r}^{\mathbf{x}} - \mathbf{r}^{\zeta}|$ does not change the order of the singularity of this term since at $(x_1 - \zeta_1) = (x_2 - \zeta_2) = 0$ this term is finite. For $M^2 > 1$, the integration is quite simple. Since both modified Bessel functions of the first kind are finite at the origin, the only singularity occurs in the second term and this remains integrable. (This is easily shown using polar coordinates.)

The convolution, Eq (2.22a), is evaluated numerically for $\psi \in [.01, 1, 100]$ and $M^2 \in [0, .5, .9, 100, 10^4]$. The modified Bessel's functions are evaluated either by using IMSL subroutines for small arguments or by using the asymptotic expressions given below for larger arguments. To find the value of the integral a two dimensional Gauss-Legendre scheme is employed. The number of integration points increased with the value of ψ.

2.4 Asymptotic Analysis of the Integration

By employing the transform

$$x_1 = \frac{z_1 - \dot{a}t}{\delta}$$

$$x_2 = \frac{z_2}{\delta}$$

in Eqs (1.1) and (1.2) the following expressions are found;

$$\frac{1}{2\psi}\nabla_{\mathbf{x}}^2 T + \frac{\partial T}{\partial x_1} = -\frac{\delta}{\dot{a}\rho c_p} S \tag{2.25a}$$

and

$$\frac{1}{2\psi}\nabla_{\mathbf{x}}^2 T - \frac{M^2}{2\psi}\frac{\partial^2 T}{\partial x_1^2} + \frac{\partial T}{\partial x_1} = -\left(\frac{\delta}{\dot{a}\rho c_p} S - \frac{M^2}{2\psi}\dot{S}\right). \tag{2.25b}$$

respectively. Note that as the parameter ψ gets large the left hand sides of both equations become more adiabatic and that the solution to the adiabatic equation is given simply as;

$$\theta_a(x_1,x_2)=\begin{cases}\frac{1}{2f}\left(1+cos(\pi\frac{x_2}{f})\right) & \text{for } x_1\le 0 \text{ and } x_2\in[-f,f],\\ \frac{1}{2f}\left(1+\cos(\pi\frac{x_2}{f})\right)(1-x_1+\frac{1}{2\pi}\sin(2\pi x_1)) & \text{for } x_1\in[0,1],\ x_2\in[-f,f],\\ 0 & \text{otherwise.}\end{cases} \tag{2.26}$$

where the temperature has been normalized by $Q\delta/\rho c_p\dot{a}$. From the definition of ψ, it is seen that one of three things may be occurring when $\psi\to\infty$: $a\to 0$, $\dot{a}\to\infty$ or $\delta\to\infty$. In Eqs (2.25a) and (2.25b) as $\psi\to\infty$ the left hand side becomes the adiabatic equation, but, depending upon how ψ is increasing, through a, $\dot{a}$ or δ, the right hand side may be affected as well. Normalizing the the temperature with respect to $Q\delta/\rho c_p\dot{a}$ in Eq. (2.24b) removes this ambiguity in the limit, and, thus, the point source term in the integrand of Eq (2.24b) rather than Eq (2.22a) is examined asymptotically for $M^2<1$.

For large arguments the modified Bessel's functions can be approximated by

$$\begin{aligned}K_0(w)&\sim\sqrt{\frac{\pi}{2w}}\exp[-w]\left\{1-\frac{1}{8w}+\frac{9}{128w^2}+\dots\right\}\\ K_1(w)&\sim\sqrt{\frac{\pi}{2w}}\exp[-w]\left\{1+\frac{3}{8w}-\frac{15}{128w^2}+\dots\right\}\end{aligned} \tag{2.27}$$

Using only the first terms, the point source in the integrand for $M^2<1$, Eq (2.24b), can be rewritten as

$$\theta_p(x_1,x_2)\sim\frac{\psi}{2\pi(1-M^2)}\sqrt{\frac{\pi}{2\psi|\mathbf{r}^{\mathbf{x}}|}}\exp\left[\frac{-\psi(x_1+|\mathbf{r}^{\mathbf{x}}|)}{1-M^2}\right]\left\{2-M^2+M^2\frac{x_1}{|\mathbf{r}^{\mathbf{x}}|}\right\} \tag{2.28}$$

where

$$|\mathbf{r}^{\mathbf{x}}|=\sqrt{x_1^2+(1-M^2)x_2^2}.$$

Given that for small x_2/x_1

$$\exp\left[-\frac{\psi}{1-M^2}|\mathbf{r}^{\mathbf{x}}|\right]\approx\exp\left[-\frac{\psi}{1-M^2}|x_1|\right]\exp\left[-\frac{\psi|x_1|}{2}\left(\frac{x_2}{x_1}\right)^2\right], \tag{2.29}$$

Eq (2.28) may be expanded to take the following form,

$$\theta_p(x_1,x_2) \sim \frac{\psi}{2\pi(1-M^2)}\sqrt{\frac{\pi}{2\psi|x_1|}}\exp\left[-\frac{\psi}{1-M^2}(x_1+|x_1|)\right]\exp\left[-\frac{\psi|x_1|}{2}\left(\frac{x_2}{x_1}\right)^2\right]$$
$$\left\{2-M^2+\mathrm{sgn}(x_1)M^2\right.$$
$$\left.-\left[\frac{2\mathrm{sgn}(x_1)M^2(1-M^2)+(2-M^2+\mathrm{sgn}(x_1)M^2)(1-M^2)}{4}\right]\left(\frac{x_2}{x_1}\right)^2\ldots.\right.$$

When $x_1 > 0$ the exponential term $\exp\left[-\psi(x_1+|x_1|)/(1-M^2)\right]$ dominates the solution and $T_p(x_1,x_2) \sim 0$; on the other hand, when $x_1 \leq 0$, $(x_1+|x_1|)=0$, the same exponential term disappears and $\mathrm{sgn}(x_1)$ is always negative. Thus,

$$\theta_p(x_1,x_2) \sim \begin{cases} \sqrt{\frac{\psi}{2\pi|x_1|}}\exp\left[-\frac{\psi}{2|x_1|}x_2^2\right]\left\{1-\frac{(1-2M^2)}{4}\left(\frac{x_2}{x_1}\right)^2+\ldots\right\} & \text{for } x_1<0; \\ 0 & \text{for } x_1>0 \end{cases} \tag{2.30}$$

It is clear that, as $\psi/2|x1|$ becomes large, the second term in the expansion becomes negligible and the solution becomes independent of M^2 Consequently, the solution for the hyperbolic heat conduction equation and the solution for the parabolic heat conduction equation converge to the same result. It is also clear that as $\psi/2|x_1| \to \infty$, $\theta_p(x_1,x_2)$ becomes, as expected from the adiabatic solution, a Dirac delta function[12] in x_2. However, contrary to the solution for the adiabatic equation and in keeping with the boundary condition $T \to \infty$ as $\mathbf{r}^{\mathbf{x}} \to \infty$, the function in Eq (2.30) loses its Dirac delta function character as $|x_1|$ grows.

Not surprisingly, similar results are found for the case $M^2 > 1$. Asymptotic analysis using the approximations

$$I_0(w) \sim \sqrt{\frac{1}{2\pi w}}\exp[w]$$
$$I_1(w) \sim \sqrt{\frac{1}{2\pi w}}\exp[w]$$

and following the same steps outlined above leads to the same leading term characterization of the solution as for the case $M^2 < 1$. Since the governing equation becomes adiabatic as the approximation becomes more accurate it is to be expected that both solutions converge to the same result as they do.

3. Results and Discussion

The solution for the simplest case, the adiabatic case in Eq (2.26), is shown in Figure 3. Behind the heat source zone the adiabatic solution is characterized by contours of constant temperature extending from the heat source zone to $x_1 = -\infty$ parallel to the crack faces. In front of the crack tip, in the heat source zone, the gradient of temperature along lines extending radially from the crack tip appears to be constant. Although it isn't true mathematically that the radial gradient in the heat source zone is constant, it is noted that the expression for the zone used here is an approximation to the experimental data and that "averaging"in the experiments due to the finite infrared detector size reduces the accuracy of the measurements near the crack tip.[2] Generally, it is expected that if adiabatic conditions prevail at the crack tip, a nearly constant radial gradient may be recorded experimentally. Good quantitative agreement is found between the predicted temperature rise and the measured temperature rise. A maximum temperature rise of 298°C is seen in the experiment when $\dot{a}$ =600 m/s, and the predicted result, 304°C occurring along the crack line, is very close to that measurement. The minimum temperature is 0°C occurring everywhere outside—except directly behind—the heat source zone.

The results of the numerical integration for the $M^2 < 1$ cases are plotted in Figures 4 through 6. For small ψ it can be seen in Figure 4 that there is a marked dependence of the temperature field upon M^2. Most notably, for $M^2 \in [.5..9]$ a region of temperature drop is seen behind the source zone. This is an interesting but unrealistic effect since the combination of parameters in these plots, $\psi = .01$ and $M^2 \in [.5..9]$, is unlikely to be seen experimentally. As $M^2 \rightarrow 1$ the temperature field becomes more localized near the origin and the temperature at any given point behind the heat source zone decreases with increasing M^2. For $M^2 = 0$ the maximum normalized temperature, θ_{max}, occurs roughly at the maximum of the heat source zone and is equal to .1% of the adiabatic maximum. The minimum, naturally, is zero as $r \rightarrow \infty$. For $M^2 = .5$ the maximum is moved forward to roughly the location of the minimum slope of the source zone where θ_{max} is equal to 1% of the adiabatic maximum. The minimum occurs roughly at the location of the maximum slope of the source zone where the normalized temperature is equal to -1% of the maximum adiabatic temperature. For the case $M^2 = .9$ the location of the maximum and minimum are not changed with respect to the case $M^2 = .5$ but the magnitude does, θ_{max} is equal to 10% of the adiabatic maximum while θ_{min} is equal to -10% of the adiabatic maximum. The behavior seen for the two cases when $M^2 \neq 0$ is exactly as expected

from Eqs (2.13) and (2.12). When $M^2 \neq 0$ there is a contribution due to the slope of the heat source zone as seen in Eq (2.13). This contribution has a cooling effect when the slope is a maximum and a heat effect when the slope is a minimum; as $M^2 \rightarrow 1$ the significance of the heating and cooling due to the modified Bessel's function of the first order becomes greater and more dominant. Thus, as $M^2 \rightarrow 1$, the maximum temperature moves to the location of minimum slope and the minimum temperature moves to the location of the maximum slope. Both maximum and minimum increase in magnitude as $M^2 \rightarrow 1$.

For larger ψ, Figure 5, the dependence of the temperature field upon M^2 begins to disappear. No negative temperature changes are seen, however, when $M^2 = .9$ the temperature does exhibit a positive minimum near the tail end of the heat source zone. Thus, some cooling effects due to the second source term in Eq (2.13) remain. Although, far from the heat source zone, $x_1/\delta > 1$, all three fields are equal. As $M^2 \rightarrow 1$ a localization of the temperature near the source zone is still seen. The maximum temperature is located near the maximum of the source function in each sub-case although it moves forward slightly as the thermal mach number increases. The maximum normalized temperature increases with thermal mach number; $\theta_{max} = .75, 1, 1.5$ for $M^2 = 0, .5, .9$ respectively. These values are 3.25%, 5% and 7.5% of the maximum temperature under adiabatic conditions.

For even larger ψ, Figure 6, the dependence upon M^2 disappears completely as expected from the asymptotic analysis, Eq (2.30), and the hyperbolic heat conduction solution is indistinguishable from the solution for parabolic heat conduction at all values of $M^2 < 1$. No localization of the temperature near the heat source zone is discernable. The maximum temperature occurs slightly behind the maximum of the heat source zone with value of 7.5—32.5% of the maximum temperature under adiabatic conditions.

Small ψ accounts for; a small source zone, δ, low velocity, $\dot{a}$, or a large thermal diffusivity, α. (See Eq (2.22b).) For metals these conditions do not reflect the usual experimental conditions. For 4340 steel, $\alpha = 10^{-5}$, and $\dot{a}\delta \approx 2$ for both experiments shown in Figure 1 giving $\psi \sim 10^5$ in both cases. For comparison the results of the integration for $\psi = 10^5$ have been plotted in Figure 7. It is seen that the theoretical temperature field matches the experimental results, Figure 1, well for $\dot{a} = 600$ m/s and that both the theoretical temperature field and the experimental temperature field resemble the adiabatic solution, Figure 3. Contours extend from the heat source zone nearly parallel to the crack faces toward $x_1 = -\infty$ before curving in to meet the negative x_1 axis.

The results for $\psi = 10^5$ differ from the adiabatic solution in that the temperature decreases as $|x_1|$ increases behind the heat source zone. It is reiterated that this decrease is expected due to the zero temperature boundary condition at $|x_1| = \infty$. This boundary condition more closely approximates the experimental condition than an adiabatic boundary condition because there is, after all, a small but significant amount of heat conduction leading to a cooling of the specimen as $|x_1| \rightarrow \infty$. It is noted that the temperature decreases more rapidly behind the crack tip in the experiments than in the theory. This is attributed to heat loss by radiation and convection at the surface. Kuang and Alturi[16] have included these effects in there numerical parabolic heat conduction analysis, and they report a more rapid decrease in the temperature behind the crack than when radiation and convection are *not* neglected. For $\dot{a} = 900$ m/s in Figure 1 a discrepancy with the theoretical results for $M^2 < 1$ in Figure 7 is seen. The contours seen experimentally emanate from the source zone outwardly before curving in to meet the negative x_1 axis. (The predicted maximum temperature at the crack tip is in good agreement with the experimental measurement, however, owing to the adiabatic conditions at the crack tip.)

For $M^2 > 1$ an exemplary plot is shown in Figure 8. The resemblance of this figure to the results recorded in Fig 1 for $\dot{a} = 900$ m/s is striking, however, the experimental temperature field for $\dot{a} = 900$ m/s shows what might be interpreted to be thermal shocks at a shock angle corresponding to a large mach number, $M \approx 100$. If this value for M is accurate then when $\dot{a} = 600$ m/s the temperature field should also show similar thermal shocks; it doesn't. Also, because $\psi = 10^5$ experimentally not 10^3 as in Fig 8, the theoretical temperature field for thermally super-sonic crack propagation at $\dot{a} = 900$ m/s actually resembles the temperature field in Fig 7. This is expected from the asymptotic analysis and has been checked numerically by the authors. Therefore, it is clear that no evidence of thermally super-sonic crack propagation is observed in these experiments.

The difference in between the experimentally observed temperature field at $\dot{a}$ =900 m/s and the predicted field at the same crack speed is due to crack face opening[3]. The opening velocity required to produce the observed effect is 7.5 m/s, a reasonable crack opening velocity. It is expected that the crack face opening speed depends upon the initial static stress intensity factor and the crack velocity. From simple theory one might expect that the crack face opening velocity increases by as much as 5 times when the crack speed increases from 600 m/s to 900 m/s.[17] This suffices to explain the difference in the temperature fields in Figures 1 and 7.

4. Conclusions

From the asymptotic analysis of the traveling point source solution of the hyperbolic heat conduction equation, it is clear that, for crack propagation in metals when the crack speed is either lower or higher than the material heat propagation speed, the difference between hyperbolic heat conduction and parabolic heat conduction is negligible (See Figures 6 and Figure 7). As the factor $\psi = \dot{a}\delta/2\alpha$ gets large, ($\psi \sim 10^5$ for a crack propagating in 4340) solutions for a traveling point source in a hyperbolic or parabolic material converge to the same result. This end result is insensitive to changes in the thermal mach number, M, and is very similar to the solution for a traveling source zone in an adiabatic material.

The temperature field in Figure 1 exhibits quasi-adiabatic heat conduction behavior when $\dot{a} = 600$ m/s. Contours of constant temperature extend from the crack tip to $|x_1| = -\infty$ nearly parallel to the crack faces before curving in to meet the negative x_1 axis. A region of nearly constant radial temperature gradient is observed ahead of the crack tip. The temperature field greatly resembles the solution for adiabatic conditions due to the high crack velocity, $\dot{a}$, small heat production zone, δ, and low thermal diffusivity, α, of 4340 steel.

When $\dot{a} = 900$ m/s the temperature field does not show behavior that is predicted by parabolic or hyperbolic heat conduction. It is understood that this difference is due to opening of the crack faces behind the crack tip.[3] Thus, no evidence of hyperbolic heat conduction is observed, and it is concluded that the traveling point source shows little promise as an experimental method for the investigation of the hyperbolic heat conduction effect. A feasible source zone size combined with the normal range of material parameters for engineering materials consistently leads to near adiabatic conditions around the source zone unless a very low thermal wave speed is expected ($\sim$ 1 m/s).

Acknowledgements

We are grateful to Office of Naval Research for support under grant N00014-90-J-1340 and to A.T. Zehnder for sharing the raw data from his investigation. The computations described here were carried out on a Cray Y-MP at the San Diego Supercomputing Center (SDSC).

References

1. A.T. Zehnder and A.J. Rosakis, On the temperature distribution at the vicinity of dynamically propagating cracks in 4340 steel, *J. Mech. Phys. Sol.*, **39**, No. 3., 385-415, (1991)

2. A.T. Zehnder and J.A. Kallivayalil, Temperature rise due to dynamic crack growth in beta-c titanium, in *Speckle Techniques, Birefringence Methods and Applications to Solid Mechanics*, SPIE Vol. 1554A, 48-59, (1991)

3. J.J. Mason and A.J. Rosakis, On the dependence of dynamic crack tip temperature fields in metals upon crack tip velocity and material parameters, SM Report 92-2, Graduate Aeronautics Laboratories, California Inst. of Tech., Pasadena, CA 91125, (1992)

4. D.Y. Tzou, Thermal shock waves induced by a moving crack, *J. Heat Transfer*, **112**, 21-27, (1990)

5. D.Y. Tzou, Thermal shock waves induced by a moving crack—a heat flux formulation, *Int. Heat Mass Transfer*, **33**, No. 5, 877-885, (1990)

6. P.M. Morse and H. Feshbach, *Methods of Theoretical Physics*, Vol. 1, pp. 837-859, pp. 865-869, McGraw-Hill Book Co., Inc., (1953)

7. W. Kaminski, Hyperbolic heat conduction equation for materials with a nonhomogeneous inner structure, *J. Heat Transfer*, **112**, 555-560, (1990)

8. K.J. Baumeister and T.D. Hamill, Hyperbolic heat conduction equation—a solution for the semi-infinite body problem, *J. Heat Transfer*, **91**, 543-548, (1969)

9. R. Weichert and K. Schonert, Temperature distribution produced by a moving heat source, *Q. J. Mech Appl. Math.*, **31**, Pt. 3, 363-379, (1978)

10. D.Y. Tzou, On the thermal shock wave induced by a moving heat source, *J. Heat Transfer*, **111**, 232-238, (1989)

11. D.Y. Tzou, Shock wave formation around a moving heat source in a solid with finite speed of heat propagation, *Int. J. Heat Mass Transfer*, **32**, No. 10, 1979-1987, (1989)

12. G. Arfken, *Mathematics for Physicists*, 3rd Edition, p. 912, Academic Press, Inc., New York, (1985)

13. H.S. Carslaw and J.C. Jaeger, *Conduction of Heat in Solids*, p. 267, Oxford University Press, London, (1959)

14. A. Papoulis, *The Fourier Integral and Its Applications*, McGraw Hill Book Co., Inc., New York, (1962)

15. G.F.D. Duff and D. Naylor, *Differential Equations of Applied Mathematics*, John Wiley & Sons, Inc., New York, (1966)

16. Z.-B. Kuang and S. Alturi, Temperature field due to a moving heat source: a moving mesh finite element analysis, *J. Appl. Mech.*, **52**, 274-280, (1985)

17. L.B. Freund, A simple model of the double cantilever beam crack propagation specimen, *J. Mech.Phys. Sol.*, **25**, 69-79, (1977)

List of Figures

List of Symbols

$\mathbf{q}$	heat flux vector
k	thermal conductivity
T	temperature rise
S	heat source function
ρ	density
c_p	heat capacity
α	$k/\rho c_P$
v	thermal wave speed
$\dot{a}$	crack tip velocity
$\mathbf{z}$	stationary coordinates system
ξ	coordinates translating with the crack tip
M	thermal mach number, $\dot{a}/v$
κ	$\dot{a}/2\alpha\sqrt{\lvert 1-M^2\rvert}$
f	aspect ratio of the heat source zone
δ	size of heat source zone
Q	magnitude of heat source zone
$\mathbf{x}$	normalized coordinates translating with the crack tip
ψ	$\dot{a}\delta/2\alpha$
θ	$\rho c_p T/Q\delta$

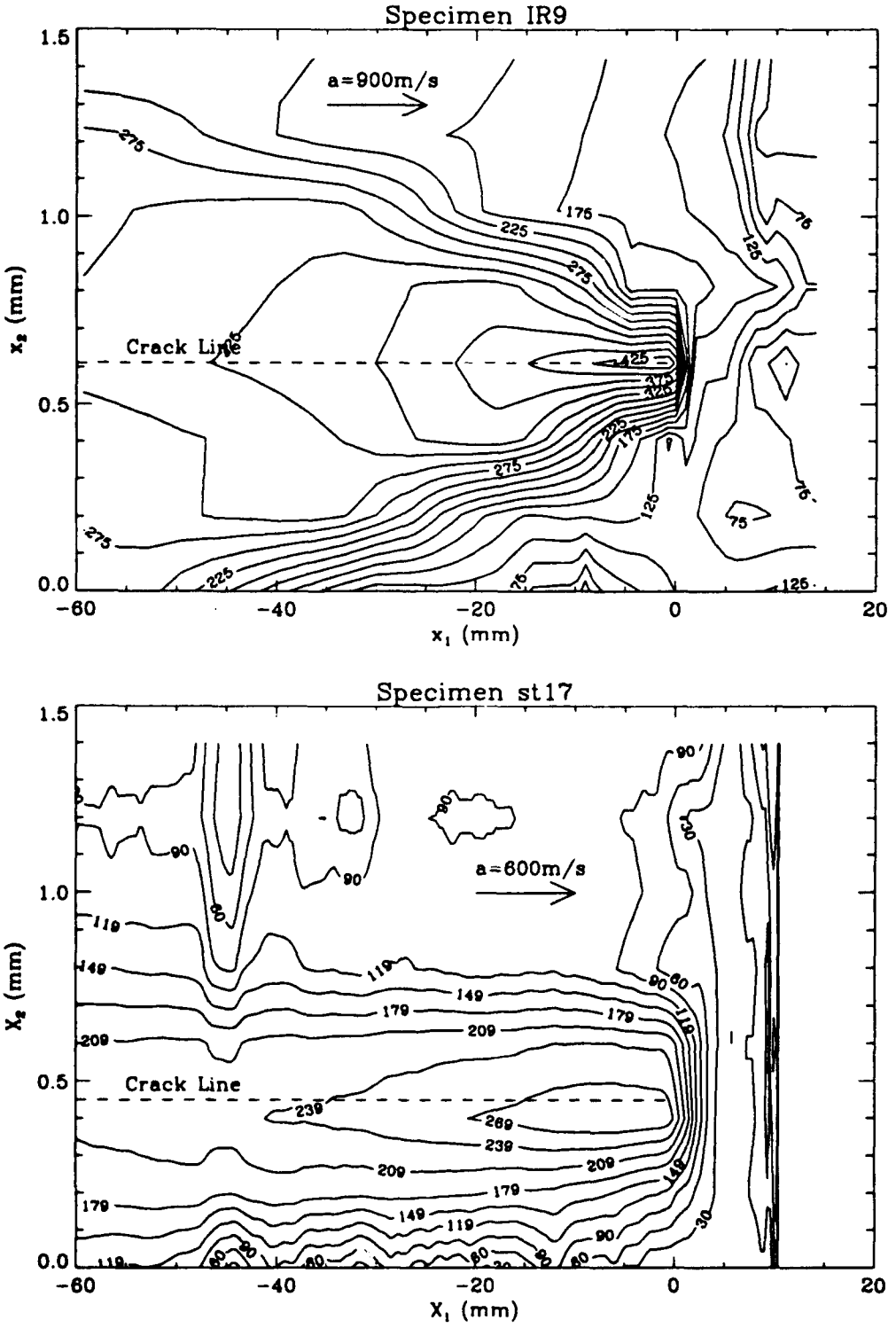
Specimen IR9
a=900m/s
Crack Line
x_2 (mm)
x_1 (mm)
Specimen st17
a=600m/s
Crack Line
X_2 (mm)
X_1 (mm)

FIGURE 1

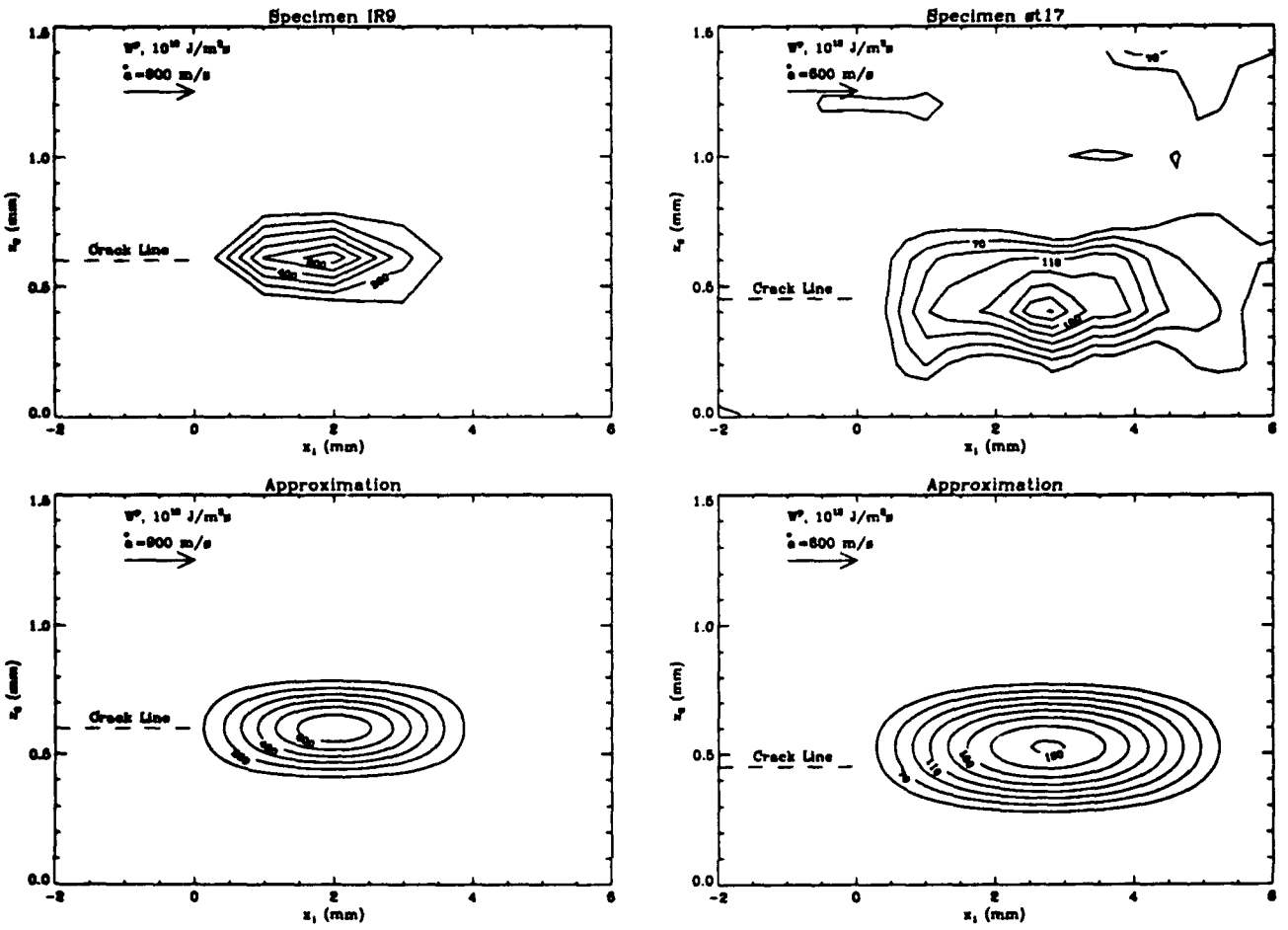
Specimen IR9
Specimen #17
Approximation
Approximation
W*, 10^10 J/m^3
ȧ=900 m/s
ȧ=600 m/s
Crack Line
x_2 (mm)
x_1 (mm)
1.5
1.0
0.5
0.0
-2
0
2
4
6
70
110
150

FIGURE 2

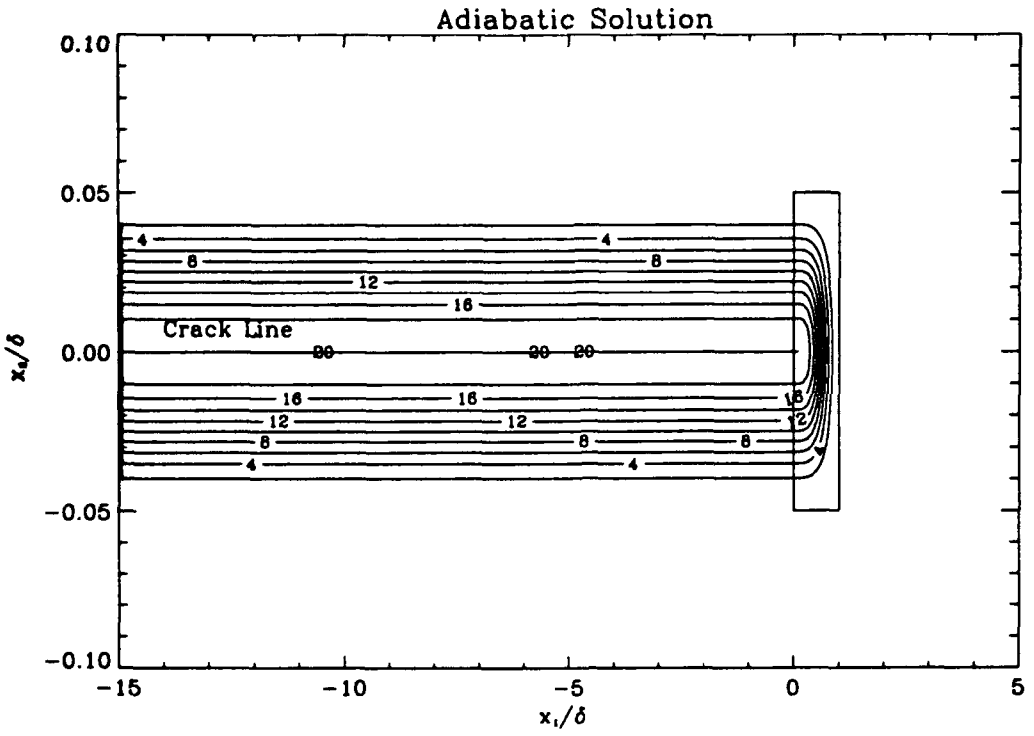
Adiabatic Solution
0.10
0.05
0.00
−0.05
−0.10
−15
−10
−5
0
5
x_2/δ
x_1/δ
Crack Line
4
8
12
16
20

FIGURE 3

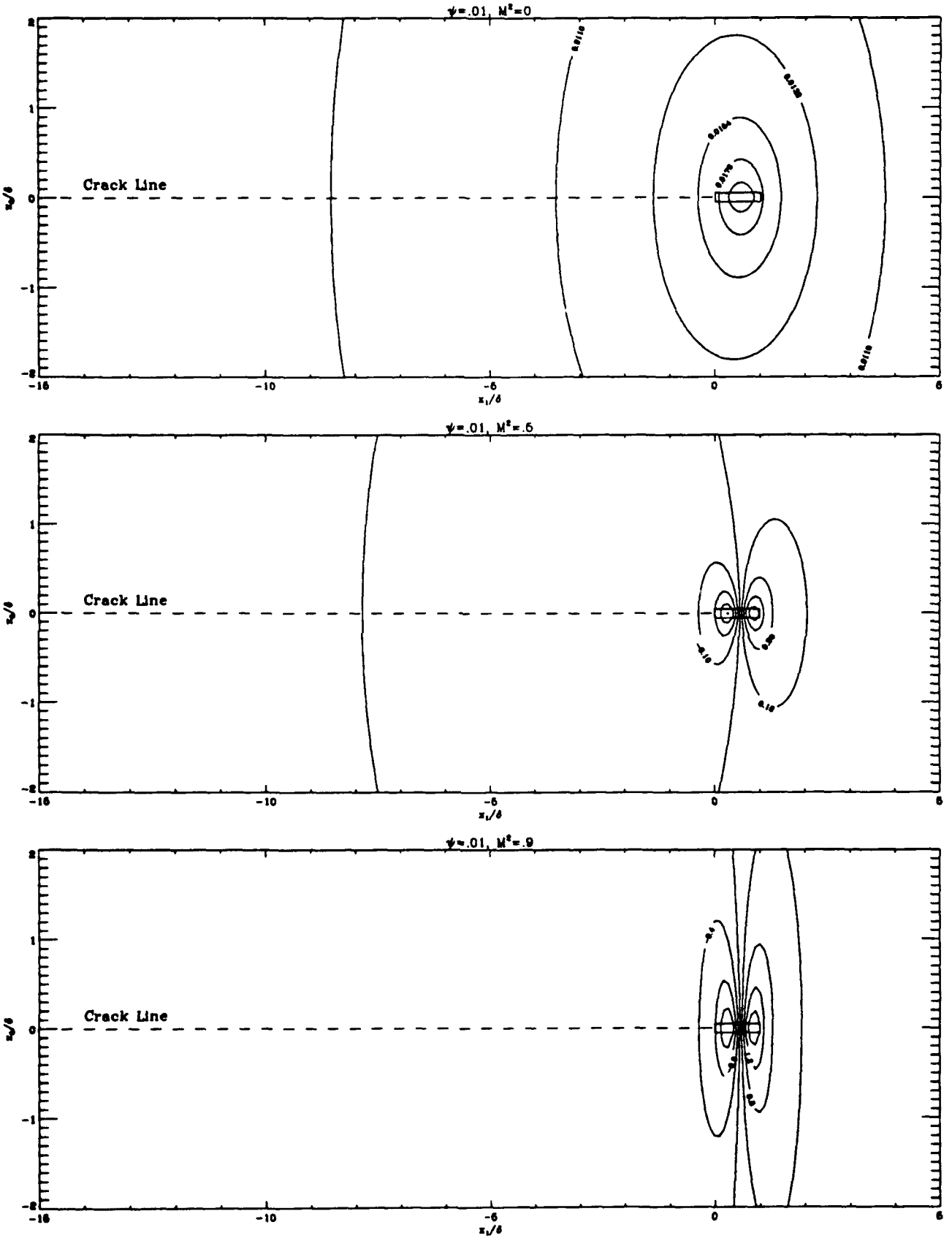
ψ=.01, M²=0
Crack Line
x₂/δ
x₁/δ
ψ=.01, M²=.6
Crack Line
x₂/δ
x₁/δ
ψ=.01, M²=.9
Crack Line
x₂/δ
x₁/δ

FIGURE 4

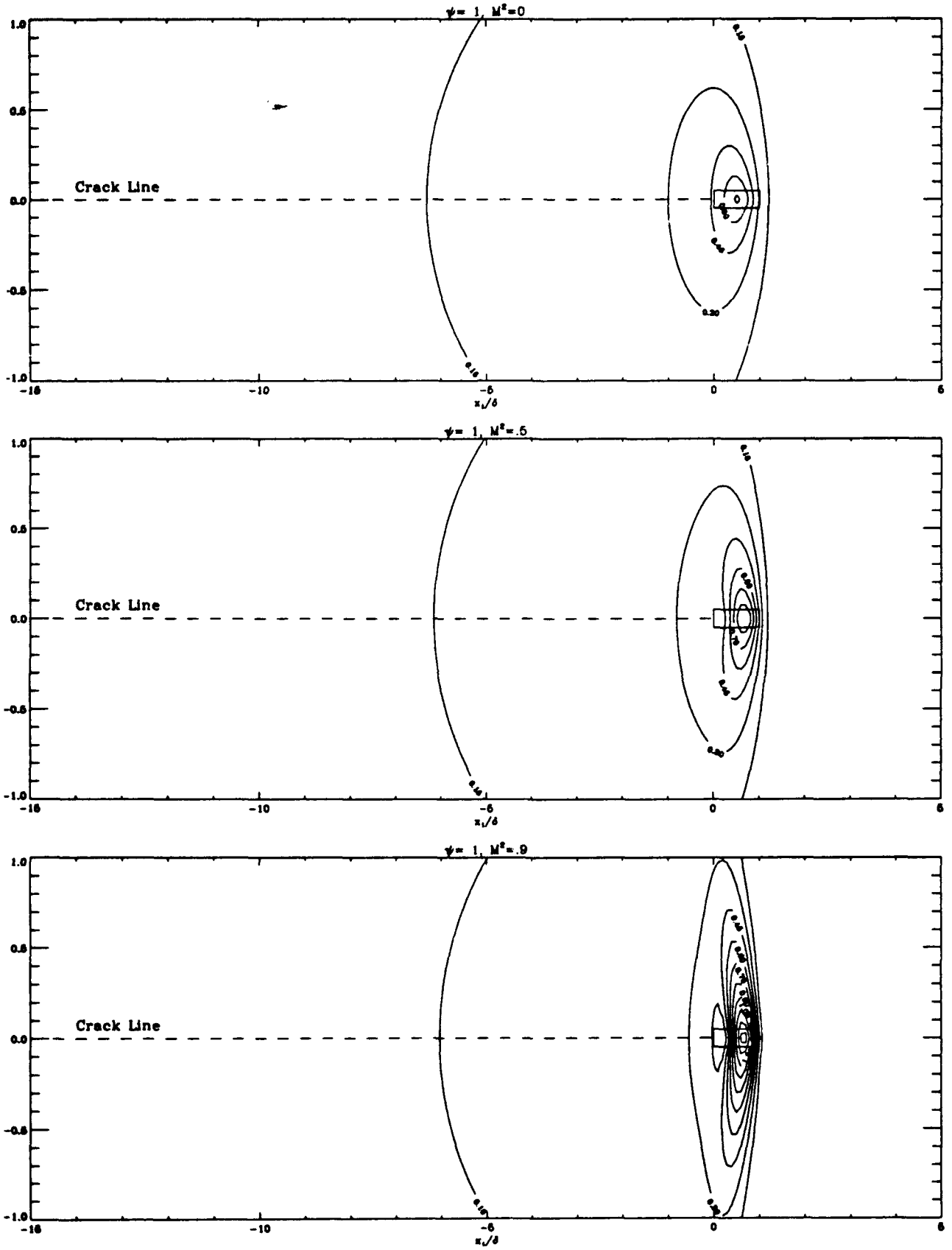

FIGURE 5

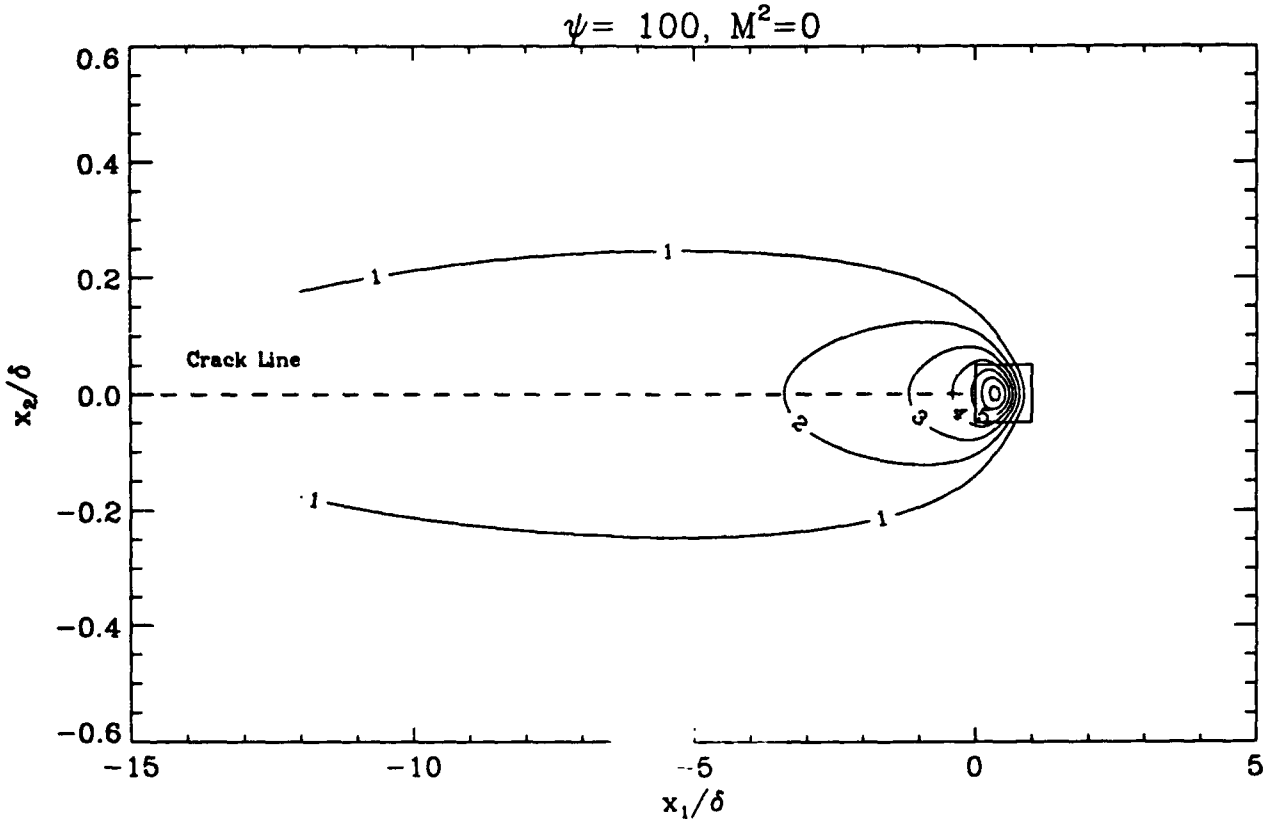
ψ= 100, M²=0
0.6
0.4
0.2
0.0
−0.2
−0.4
−0.6
x₂/δ
Crack Line
1
1
1
1
2
3
4
5
−15
−10
−5
0
5
x₁/δ

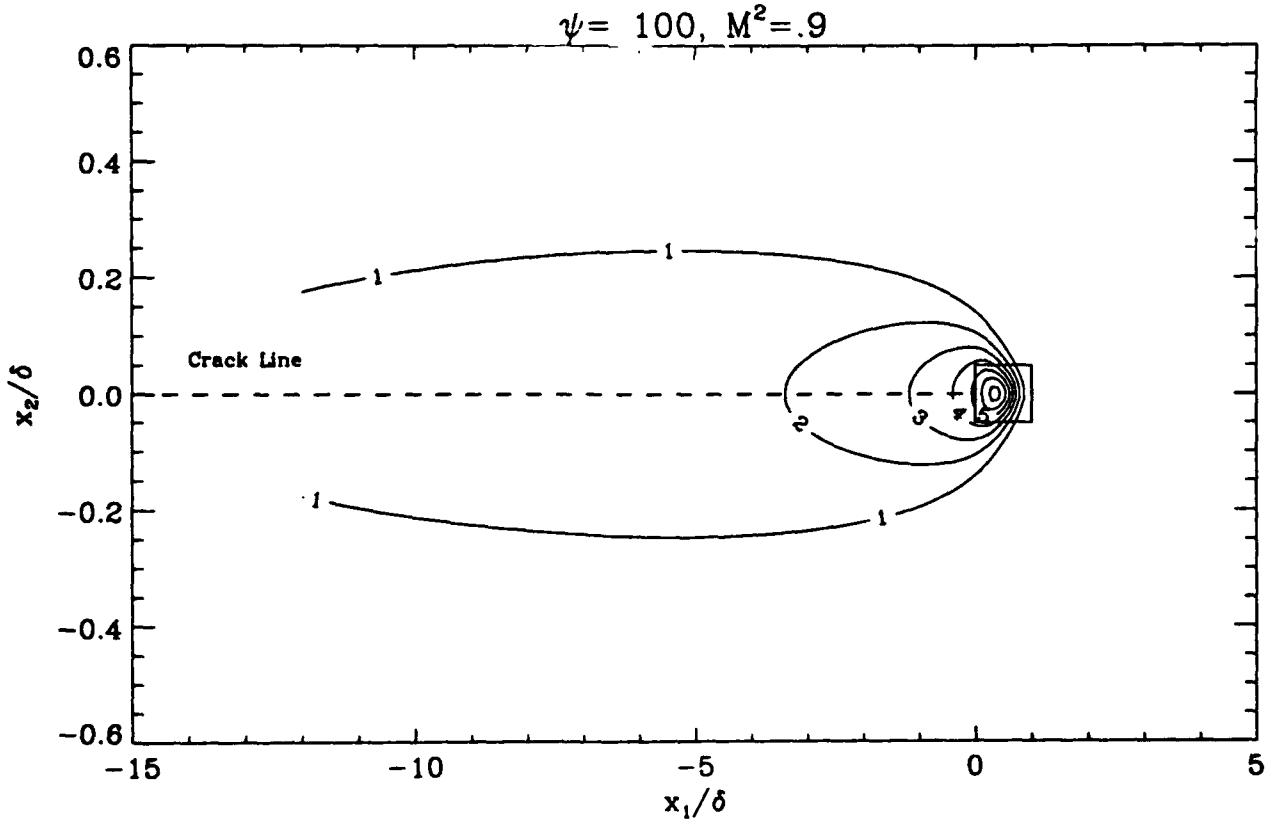
ψ= 100, M²=.9
0.6
0.4
0.2
0.0
−0.2
−0.4
−0.6
x₂/δ
Crack Line
1
1
1
1
2
3
4
5
−15
−10
−5
0
5
x₁/δ

FIGURE 6

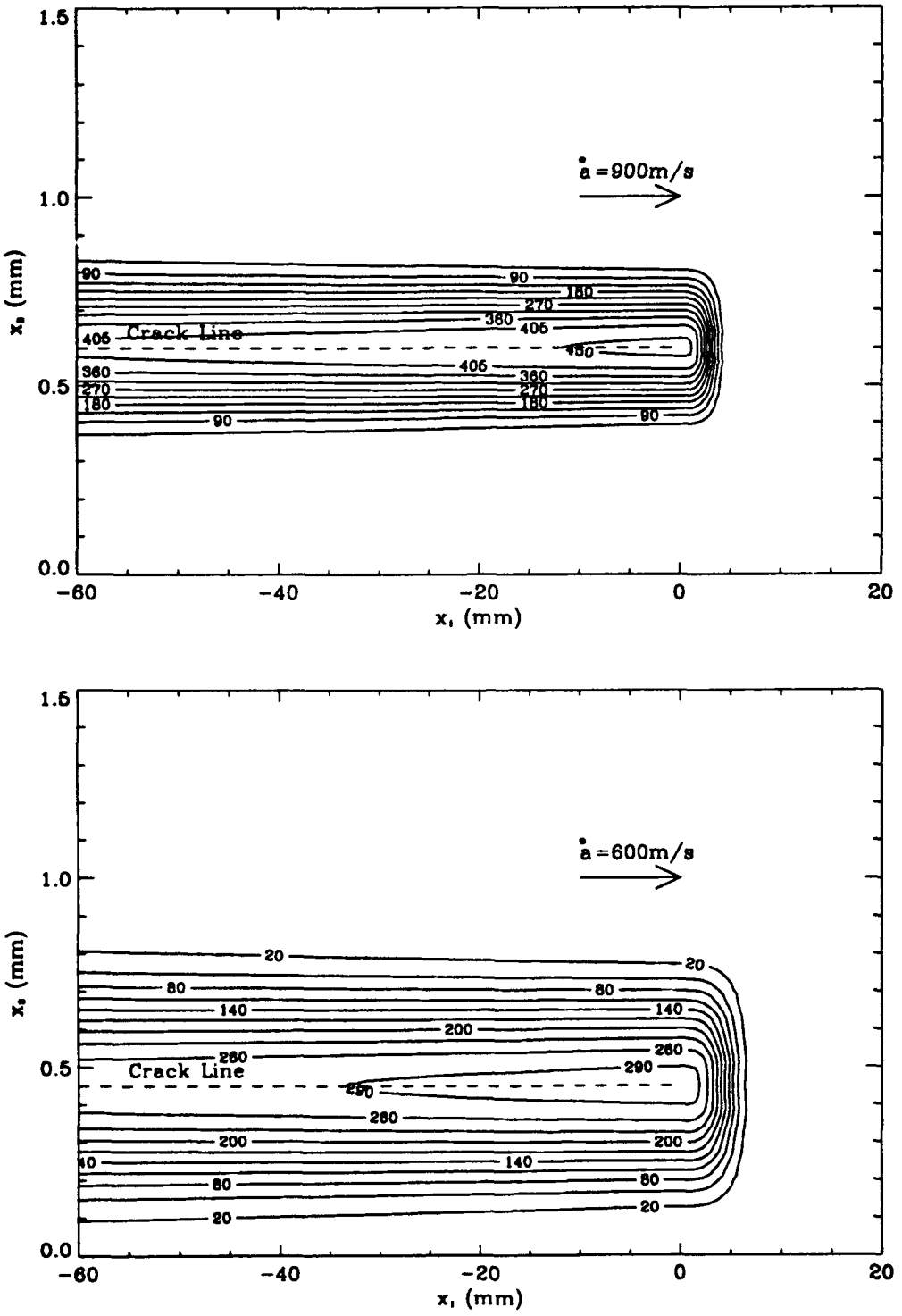
1.5
1.0
0.5
0.0
x_2 (mm)
$\dot{a}$ =900m/s
Crack Line
90
180
270
360
405
450
406
x_1 (mm)
−60
−40
−20
0
20
$\dot{a}$ =600m/s
Crack Line
20
80
140
200
260
290
250
x_1 (mm)

FIGURE 7

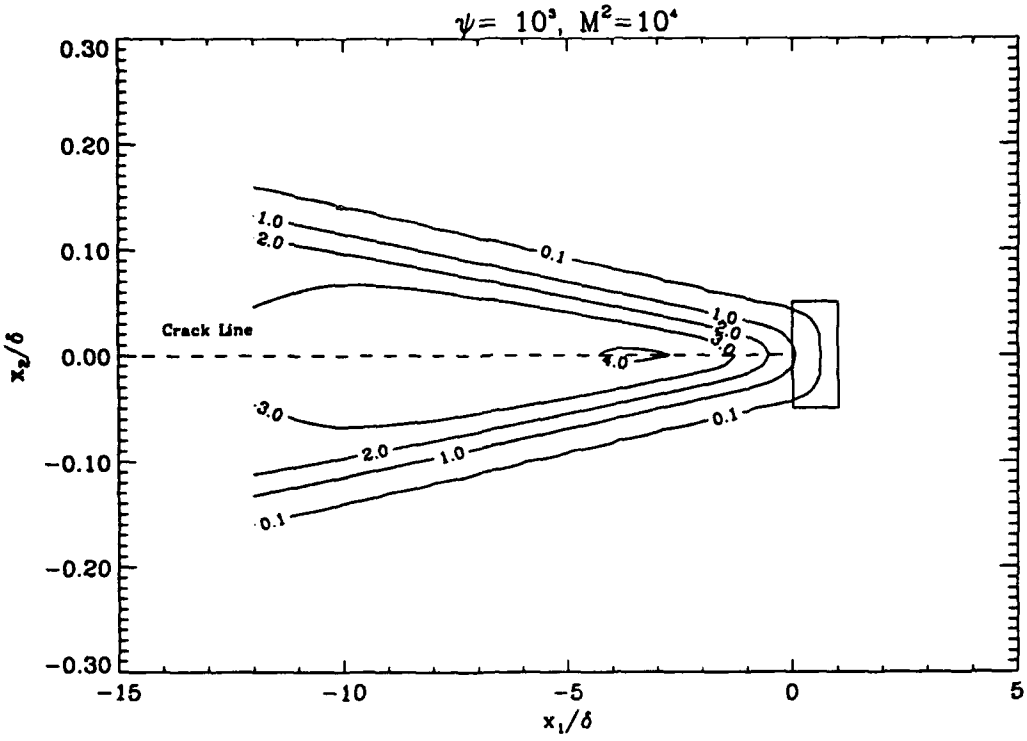
$\psi = 10^3$, $M^2 = 10^4$
0.30
0.20
0.10
0.00
−0.10
−0.20
−0.30
−15
−10
−5
0
5
x_2/δ
x_1/δ
Crack Line
1.0
2.0
0.1
1.0
2.0
1.0
2.0
0.1
2.0
1.0
0.1

FIGURE 8